Ion Trapping by Dispersed Helical Carbon Nanotubes for Accelerated Electro-Optic Switching in Liquid Crystal Devices

Rajratan Basu * and Christian C Kehr

Posted Date: 17 March 2025

doi: 10.20944/preprints202503.1164.v1

Keywords: liquid crystals; ionic impurities; helical carbon nanotubes; electro-optic effects

 doi:10.20944/preprints202503.1164.v1

Article

Ion Trapping by Dispersed Helical Carbon Nanotubes for Accelerated Electro-Optic Switching in Liquid Crystal Devices

Rajratan Basu * and Christian C. Kehr

Department of Physics, Soft Matter and Nanomaterials Laboratory, The United States Naval Academy, Annapolis, Maryland 21402, USA

* Correspondence: basu@usna.edu

Abstract: Free-ion impurities in liquid crystals (LCs) significantly impact the dynamic electro-optic performance of liquid crystal displays (LCDs), leading to slow switching times, short-term flickering, and long-term image sticking. These ionic contaminants originate from various sources, including LC cell fabrication, electrode degradation, and organic alignment layers. This study demonstrates that doping LCs with a small concentration of helical carbon nanotubes (*h*CNTs) effectively reduces free-ion concentrations by approximately 70%. The resulting reduction in ionic impurities lowers the rotational viscosity of the LC, facilitating faster electro-optic switching. Additionally, the purified LC exhibits enhanced dielectric anisotropy, further improving its performance in display applications. These findings suggest that *h*CNT doping offers a promising approach for mitigating ion-related issues in LCs without the need for additional chemical treatments, paving the way for an efficient LCD technology.

Keywords: liquid crystals; ionic impurities; helical carbon nanotubes; electro-optic effects

1. Introduction

Excess ionic impurities in liquid crystals (LCs) present significant challenges [1,2] in liquid crystal display (LCD) technology, affecting electro-optic performance through slow response times, short-term flickering, and long-term image retention (commonly known as image sticking or dead pixels) [3–9]. These free ions originate from multiple sources, including LC chemical synthesis, degradation of conductive electrodes [10,11], and polyimide (PI) alignment layers [12]. Additionally, ionic contamination can arise from the chemical decomposition and self-dissociation of LC materials [13]. Understanding the influence of free ions on the electrical, mechanical, and electro-optic properties of LCs is crucial for both fundamental research and practical applications [14–21].

Several methods exist to mitigate ionic contamination in LCs [22]. Traditional purification techniques, such as chromatography, zone refining, multiple recrystallizations, vacuum distillation, extraction, vacuum sublimation, ion exchange, and electrodialysis, are effective but often costly, time-consuming, and labor-intensive [23–26]. Furthermore, even highly purified LCs can acquire new ionic impurities during device fabrication due to interactions with electrodes, alignment layers, and adhesives [10–12]. Thus, developing alternative approaches to ion removal remains an active area of research.

Recent efforts have explored nanomaterials as an alternative to conventional chemical purification. Studies have shown that dispersing nanomaterials such as ferroelectric nanoparticles [27,28], titanium nanoparticles [29], carbon nanotubes [30–32], graphene [33–37], fullerenes [36,38,39], and gold nano-urchins [40] in LCs can effectively reduce free-ion concentrations via ion trapping. Additionally, two-dimensional materials like graphene [41] and hexagonal boron nitride [42,43] have demonstrated ion-capturing capabilities that enhance the overall performance of LC-based electro-optic devices.

 doi:10.20944/preprints202503.1164.v1

Helical carbon nanotubes (*h*CNTs) [44] represent a unique class of chiral materials with a distinctive spring-like morphology, high modulus, and superior electronic properties compared to conventional graphite structures [45,46]. This study demonstrates that doping LCs with a small concentration of *h*CNTs results in a substantial (~70%) reduction of free ions. The trapping mechanism is attributed to the anisotropic, spring-like outer surface of the *h*CNTs, which effectively captures ionic impurities. Experimental results reveal that this ion reduction leads to notable changes in the intrinsic properties of the LC, including decreased rotational viscosity, improved electro-optic switching dynamics, and enhanced dielectric anisotropy. These findings highlight the potential of *h*CNTs as a promising solution for mitigating ion-related issues in LCs without the need for extensive chemical purification.

2. Materials

In this study, non-functionalized helical multiwalled carbon nanotubes (*h*CNTs) in powder form, obtained from US Research Nanomaterials, Inc. (USA), were utilized to investigate their effect on ionic impurity reduction and electro-optic behavior in a nematic LC system. The *h*CNTs had an outer diameter of 130 nm and an average length of 6 μm. Figure 1(a) is an SEM image of hCNTs.

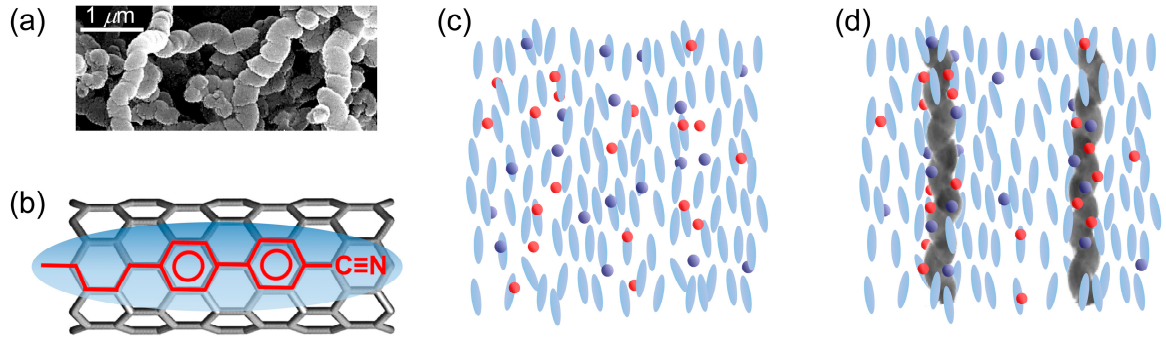

Figure 1. (a) An SEM image of *h*CNTs. (b) A schematic illustration of LC-CNT interaction: anchoring of an LC molecule on a regular CNT surface due to π–π electron stacking. The blue ellipsoid is a generic LC molecule, and the black cylindrical honeycomb structure is a CNT surface. (c) Random distribution of free ions in a nematic phase. (d) *h*CNTs' ion trapping process in a nematic phase.

The *h*CNTs were initially dispersed in ethanol to ensure uniform dispersion of *h*CNTs in the LC medium. The ethanol+*h*CNTs suspension was first shaken using a vortex mixer for 1 h and subsequently sonicated for 6 h. The nematic LC E7 (EMD Millipore Corporation, T_{NI} = 60°C) was then added to the ethanol+*h*CNTs mixture and sonicated for an additional hour to achieve complete dissolution. The ethanol was slowly evaporated at an elevated temperature, leaving behind a purified E7+*h*CNTs mixture with a final *h*CNT concentration of approximately 3.1 × 10^{-3} wt.%. To eliminate residual solvent and air bubbles, the mixture was degassed under vacuum for 4 h, followed by further sonication for 6 h.

For consistency, the pure LC E7 was subjected to the same treatment process—dissolution in ethanol, controlled evaporation, and degassing—before experimental analysis. The LC E7 and E7+*h*CNTs mixture were then introduced into commercially manufactured antiparallel-rubbed planar LC cells (Instec, Inc., USA), featuring an indium tin oxide (ITO)-coated area of 1 × 1 cm^2 and a cell gap of d = 20 ± 0.20 μm. The conventional optical interferometric measurement was employed to measure the cell thickness precisely using the equation, $d = k\,\lambda_1\,\lambda_2/2(\lambda_2 - \lambda_1)$ where k is the number of interference cycles between wavelengths λ_1 and λ_2. The cells were filled via capillary action at an elevated temperature (T = 65°C) in the isotropic phase and subsequently cooled to room temperature for characterization.

 doi:10.20944/preprints202503.1164.v1

It is well established that LC molecules anchor to the surface of *regular* CNTs via π–π stacking interactions, maximizing the hexagon–hexagon interaction between the benzene rings of the LC molecules and the honeycomb lattice of the CNTs [47]. This interaction is schematically illustrated in Figure 1(b), where the ellipsoid represents a generic LC molecule, and the black cylindrical structure denotes the CNT surface. The molecular structure of a representative LC molecule is depicted within the ellipsoid, positioned on the CNT surface to highlight the π–π electron stacking interaction. This interaction is characterized by the alignment of the benzene rings of the LC molecules with the hexagonal lattice of the CNTs. The anchoring energy associated with this π–π stacking interaction is estimated to be $|U_{\text{anchor}}| \approx 2.0$ eV per molecule [47]. When CNTs are dispersed as colloidal inclusions in an LC medium, this π–π stacking interaction drives the CNTs to align along the nematic director while simultaneously inducing the LC molecules to orient along the CNT long axis on the CNT surface [48–51]. This stable anchoring mechanism leads to several intriguing phenomena, including an enhancement of the nematic orientational order parameter in LCs [50], the formation of pseudo-nematic LC domains around the CNTs even in the isotropic phase [51,52], the transfer of CNT surface chirality to otherwise achiral LCs [53–57], an increase in the polar anchoring energy at the LC-CNT interface [58], and vertically aligned CNTs-induced homeotropic LC alignment [59,60].

All those prior studies have focused on regular (non-helical) CNTs. The findings presented in this work demonstrate the potential of *h*CNTs as a promising approach for mitigating ion-related issues in LCs without necessitating extensive chemical purification. Figure 1(c) schematically shows the presence of ions in a nematic phase. Figure 1(d) schematically shows the ion trapping phenomenon by the dispersed *h*CNTs in the LC.

3. Experiments, Results, and Discussions

3.1. Ion Concentration

The free-ion concentration, n_i, in LC E7 and E7+hCNTs, was determined by analyzing the transient ion current, I_{ion}, generated upon inverting the polarity of the applied voltage across the cell [28,61]. When a square-wave voltage alternates between +V and −V, the LC molecules do not undergo director rotation since their reorientation depends solely on the magnitude of the electric field E, not its polarity [62]. However, the inversion of voltage polarity induces the migration of free ions toward the opposite electrodes, resulting in a transient ion current, I_{ion}, within the LC cell.

To generate I_{ion}, a square-wave voltage with a peak-to-peak amplitude of 30 V (ranging from +15V to −15V) at 1 Hz was applied using an Automatic Liquid Crystal Tester (Instec, Inc.). The resulting ion current as a function of time was recorded at T= 25°C, as shown in the inset in Figure 2. The transient ion current reaches its peak value when the positive and negative ions meet approximately at the center of the cell. The peak time, is given by: $t_{ion-peak} = \frac{d^2}{2\mu E}$, where μ is the ion mobility [61]. As the ions continue their migration, I_{ion} eventually decays to zero when they reach the opposite electrodes, as observed in the inset in Figure 2. The total free-ion transport was calculated by integrating the area under the I_{ion} vs. time curve, and the free-ion concentration was extracted using: $n_i = (\int_0^t I_{ion} dt)/A.d$, where A is the active electrode area, and d is the cell gap. At elevated temperatures, both the free-ion concentration and ion mobility increase. Figure 2 shows n_i for both samples as a function of temperature, revealing a substantial suppression of ion concentration in E7+hCNTs compared to pure E7. Notably, for the E7+hCNTs sample, n_i is reduced by approximately 60% to 70% in the temperature range, 25°C to 60 °C.

 doi:10.20944/preprints202503.1164.v1

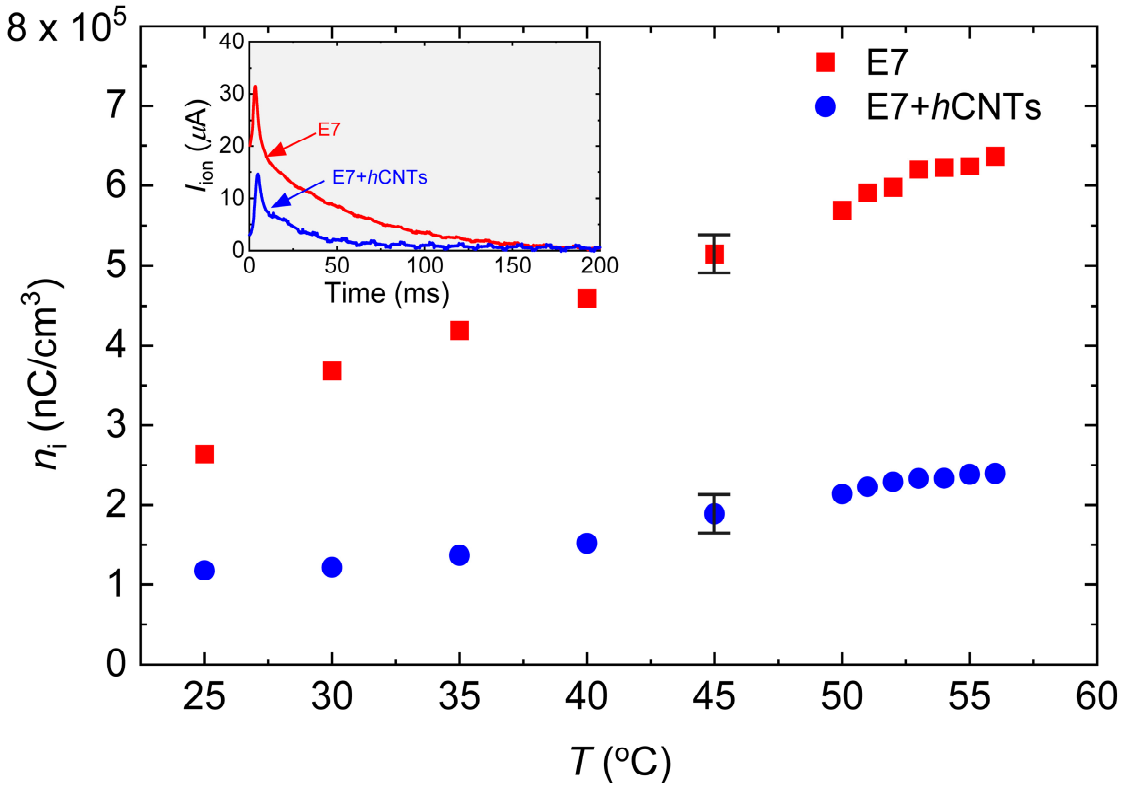

Figure 2. Free ion concentration, n_i, as a function of temperature for E7 and E7+*h*CNTs samples listed in the legend. Typical error bars are shown. Inset: Ion current, I_{ion} as a function of time for E7, E7+*h*CNTs at 25 °C after the voltage is inverted across the cells. The peak represents the ion bump when positive and negative ions meet in the middle of the cell.

Literature reports [63] indicate that non-helical CNTs at a concentration of 0.05 wt.% reduce the ion concentration in liquid crystal E7 by approximately 50% at 30°C. However, at temperatures exceeding 45°C, this reduction decreases to around 20% or less [63]. In the present study, hCNTs at an ultralow concentration of ~10^{-3} wt.% achieved a reduction in ion concentration exceeding 65% over a broad temperature range. Since no known attractive force exists between hCNTs and free ions, this enhanced ion trapping is likely facilitated by the asymmetric spring-like morphology of hCNT-walls, which effectively capture both positive and negative ions within the LC.

The ion-trapping efficiency of hCNTs can be better understood by comparing it with other nanomaterials reported in the literature. Previous studies have demonstrated that different nanoparticles exhibit varying degrees of ion-trapping capabilities in liquid crystals. For instance, graphene nanoplatelets at a concentration of 0.5 wt.% in LC 8OCB resulted in a 30% reduction in ion concentration [22], while a similar concentration of graphene platelets in cholesteric LCs led to an approximately 32% reduction [22]. A much higher efficiency was observed in ferroelectric LCs doped with 0.5 wt.% fullerenes (C_{60}), where an 80% decrease in ion concentration was reported [64]. Ferroelectric $BaTiO_3$ nanoparticles, when incorporated at 0.275 wt.% in LC 5CB, were found to trap about 50% of the free ions [28]. In another study [22], titanium dioxide (TiO_2) nanoparticles at a concentration of 0.1 wt% were observed to reduce ion impurities in LC E7 by 53%.

Thus, the ion trapping by hCNTs in the current study is comparable to, or in some cases even exceeds, that of other nanomaterials reported in prior studies. However, what sets hCNTs apart is their ability to achieve a significant reduction in ion concentration at substantially lower doping concentrations than other nanoparticles.

 doi:10.20944/preprints202503.1164.v1

3.2. Rotational Viscosity

The rotational viscosity, γ_1, of an aligned LC quantifies the internal friction among LC molecules during their rotational motion. To investigate γ_1 in our LC samples, we conducted experiments using the same planar-aligned capacitive cell configuration, where the transient current induced by a DC field was measured [65–67]. When a DC field, significantly exceeding the threshold field, is applied across the LC cell, the induced current I(t) exhibits a characteristic time response as the nematic director undergoes dynamic rotation. The time-dependent current response follows the relation

$$I(t) = \frac{A\,(\Delta\varepsilon\,\varepsilon_o)^2\,E^3}{\gamma_1} sin^2\,[2\theta(t)] \quad (1)$$

where A is the area of the cell, E is the applied electric field, $\Delta\varepsilon$ is the dielectric anisotropy, ε_0 is the free space permittivity, and θ represents the director angle relative to the electrodes at a given time. The peak current occurs at $\theta = 45^o$, yielding

$$I_p = \frac{A\,(\Delta\varepsilon\,\varepsilon_o)^2\,E^3}{\gamma_1} \quad (2)$$

at the peak time,

$$t_p = [\frac{\gamma_1(-ln\,(tan\,\theta_o))}{\Delta\varepsilon\,\varepsilon_o}]\frac{1}{E^2} \quad (3)$$

where θ_o is the pre-tilt angle. A DC voltage pulse of 35 V with a 1 Hz interval was applied across the cell to generate $I(t)$, which was subsequently detected as a function of time via a digital storage oscilloscope through a load resistor in series. The inset in Figure 3 presents an example of $I(t)$ for two test cells, E7 and E7+*h*CNTs, at T= 25°C. The peak current I_p was extracted from the $I(t)$ versus time graph, and γ_1 was determined using the known values of E, $\Delta\varepsilon$, and A. The method for measuring $\Delta\varepsilon$ is discussed later.

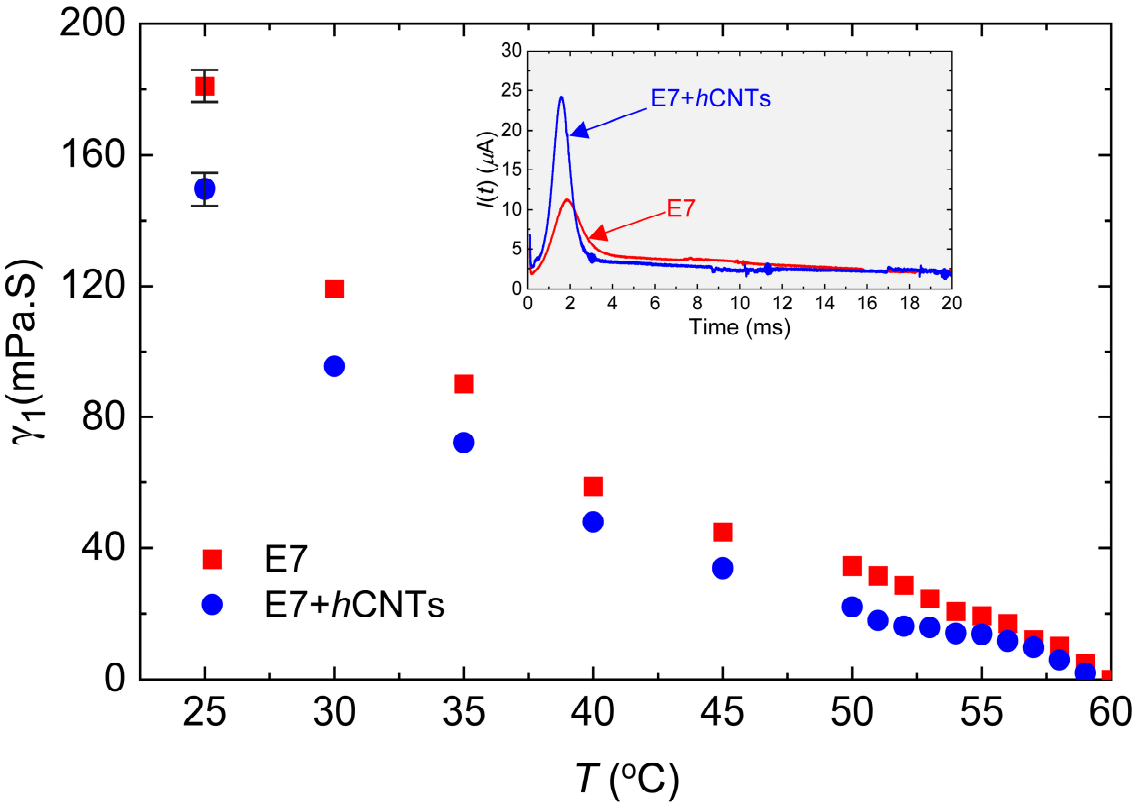

 doi:10.20944/preprints202503.1164.v1

Figure 3. Rotational viscosity, γ_1 as a function of temperature for E7 and E7+*h*CNTs samples, listed in the legend. Typical error bars are shown. Inset: Transient current, I(t) as a function of time for E7 and E7+*h*CNTs at T = 25°C. .

Figure 3 depicts γ_1 as a function of temperature for the two cells. A clear pre-transitional behavior is observed for both samples, with E7+*h*CNTs exhibiting a significant reduction in γ_1 compared to pure E7. The reduction in γ_1 for the E7+*h*CNTs sample is approximately 17% at T = 25 °C.

Previous studies have suggested that the suppression of ionic impurities can lead to a decrease in the rotational viscosity of an LC. For instance, quantum dot-doped LCs have been shown to exhibit reduced γ_1 due to the trapping of ionic impurities, which lowers the overall ionic density and resistance of the nematic medium [68]. Similarly, our group previously reported that graphene flakes in a ferroelectric LC reduce rotational viscosity by effectively trapping ionic impurities [33]. Another study demonstrated that titanium nanoparticles suppress free ions, leading to stronger van der Waals dispersion interactions between LC molecules and the alignment layers, thereby reducing the pre-tilt angle of the LC molecules [29]. According to Eq. (3), $\gamma_1 \propto 1/(-ln\,(tan\,\theta_o))$, for a constant applied field, implying that a decrease in the pre-tilt angle, θ_o, results in a corresponding decrease in γ_1. In our study, we attribute the observed reduction in γ_1 for the E7+*h*CNTs sample to the suppression of ionic impurities. The decrease in internal resistance and friction, coupled with enhanced van der Waals interactions between LC molecules and the alignment layers, likely leads to a reduction in the pre-tilt angle, thereby decreasing γ_1. While a direct quantitative theoretical model linking ion concentration to γ_1 is not yet available, our findings are in agreement with previous reports, suggesting a coherent relationship between reduced ionic impurities and lower rotational viscosity.

3.3. Dielectric Anisotropy

The nematic phase exhibits dielectric anisotropy, defined as $\Delta\varepsilon=\varepsilon_{\parallel}-\varepsilon_{\perp}$, $\varepsilon_{\parallel}$ and $\varepsilon_{\perp}$ are the dielectric permittivities parallel and perpendicular to the nematic director, respectively. To measure the dielectric constant ε as a function of the electric field, we employed an Automatic Liquid Crystal Tester (Instec, Inc.) operating at 1000 Hz for both pure E7 and E7+hCNT samples. Figure 4(a) shows ε vs V_{rms} at 25°C. The values of $\varepsilon_{\parallel}$ and $\varepsilon_{\perp}$ were then used to determine $\Delta\varepsilon$, as described in detail elsewhere [69]. Figure 4(b) illustrates the temperature dependence of $\Delta\varepsilon$ for the two test cells. Notably, $\Delta\varepsilon$ is higher in E7+hCNTs sample.

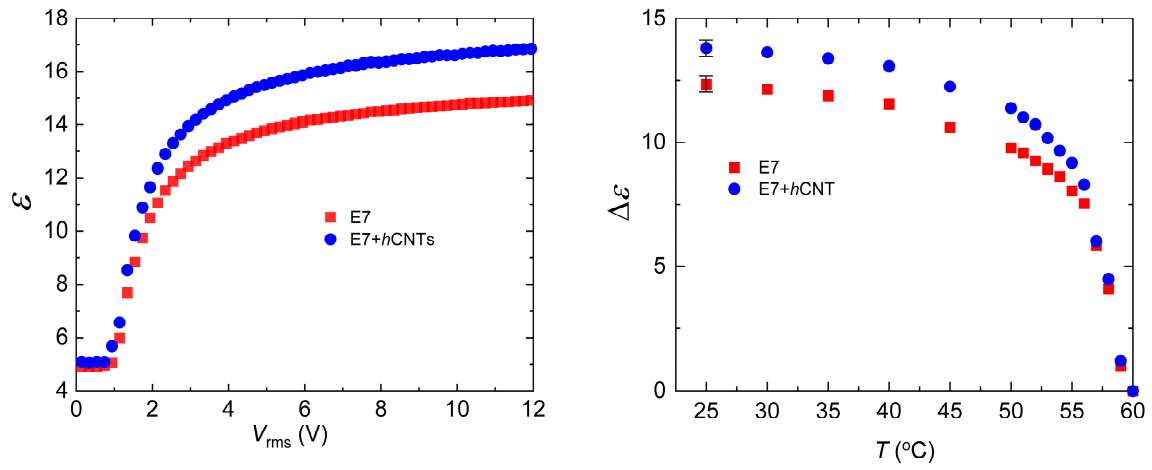

Figure 4. (a) Dielectric constant, ε as a function of V_{rms} for E7 and E7+*h*CNTs samples, listed in the legend at T = 25°C. (b) Dielectric anisotropy, $\Delta\varepsilon$ as a function of temperature for E7 and E7+*h*CNTs samples, listed in the legend. Typical error bars are shown. .

 doi:10.20944/preprints202503.1164.v1

According to Maier and Meier's theory [70], the dielectric anisotropy Δε in the nematic phase is given by

$$\Delta\varepsilon = \frac{NhFS}{\varepsilon_0}\left[\Delta\alpha + \frac{\mu^2 F}{2k_B T}(3\cos^2\beta - 1)\right] \quad (4)$$

where N is the number density of LC molecules, μ is the resultant dipole moment, $\Delta\alpha$ is the polarizability anisotropy, S is the orientational order parameter, β is the angle between the molecular long axis and the dipole moment, h is the cavity field factor, and F is the feedback factor [70].

The presence of excess ionic impurities in the LC can influence the effective dipole moment of the LC molecules. Since LC molecules possess permanent dipole moments, negatively charged ions may accumulate near the positive ends of the molecules, while positively charged ions may cluster near the negative ends. This ionic accumulation effectively reduces the net dipole moment μ, leading to a decrease in Δε according to Eq. 4. Thus, we propose that the suppression of ionic impurities in the E7+hCNTs sample enhances the effective polarity of the LC molecules, resulting in an increased Δε.

Previous studies support this interpretation. For example, it has been reported that doping a nematic LC with 0.2 wt.% TiO_2 nanoparticles increases Δε an effect attributed to the ion-trapping capability of TiO_2 [71]. Another study [68] demonstrated that doping nematic LCs with quantum dots (0.05 wt.%) captures free ions, enhancing the LC's birefringence. This suggests that suppressing ionic impurities improves the orientational order parameter S, which, in turn, leads to an increase in Δε. Our observations are consistent with these findings, further supporting the role of ion trapping in enhancing the dielectric anisotropy of liquid crystal systems.

3.4. Electro-Optic Effect

The rotational viscosity, γ_1, plays a critical role in determining the dynamic electro-optic response of aligned nematic LCs. Since γ_1 is altered in the presence of hCNTs, we investigated the dynamic electro-optic response of the E7+hCNTs composite and compared it to that of pure E7. First, Figure 5(a) shows the field-off bright state and field-on dark state with their corresponding micrographs for the E7+hCNTs composite. Then, an experimental approach, schematically shown in Figure 5 (b) was employed using an optical setup where a 5-mW He-Ne laser beam (λ = 633 nm) was directed through a polarizer, an LC cell (with the director oriented at 45° relative to the polarizer), a crossed analyzer, and a photodetector. The detected intensity was recorded using a digital storage oscilloscope to analyze the temporal variation in transmittance upon applying a modulated square-wave driving voltage at 25°C. Upon voltage application, the transmitted intensity decreases, with the optical switching-on time (τ_{on}) defined as the interval required for intensity to drop from 90% to 10% of its maximum value. Conversely, upon voltage removal, the transmitted intensity increases, with the optical switching-off time (τ_{off}) defined as the time required for intensity to rise from 10% to 90% of its maximum value. These switching times are governed by the following relations [72]:

$$\tau_{on} \propto \frac{\gamma_1}{\Delta\varepsilon\,\varepsilon_o V^2 - K_{11}\pi^2}\left(d^2 + \frac{4\,d\,K_{11}}{W_\theta}\right);\quad \tau_{off} \propto \frac{\gamma_1}{\Delta\varepsilon\,\varepsilon_o V_b^2 - K_{11}\pi^2}\left(d^2 + \frac{4\,d\,K_{11}}{W_\theta}\right) \quad (5)$$

were d represents the cell gap, Δε is the dielectric anisotropy, V (>>V_{th}) is the driving applied voltage, V_b is the bias voltage, ε_0 is the permittivity of free space, K_{11} is the splay elastic constant, and W_θ is the polar anchoring strength coefficient.

Figures 5(c) illustrate the normalized transmitted intensity (left-hand y-axis) for E7 and E7+hCNTs as a function of time upon applying a modulated square-wave driving voltage (right-hand y-axis) with a $|V_b|$ = 5 V and a |V|= 25 V (>>V_{th} = 0.90 V) and f = 20 Hz).

 doi:10.20944/preprints202503.1164.v1

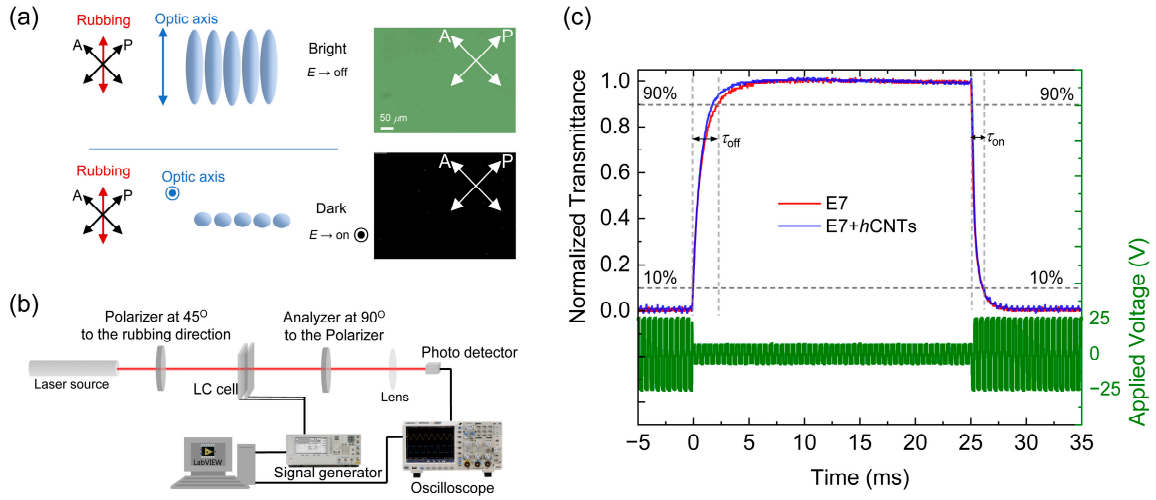

Figure 5. (a) A schematic representation of the field-off bright state and field-on dark state for a nematic LC. The micrographs for the E7+*h*CNTs cell show a field-off bright state and a field-on dark state, respectively. (b) A schematic representation of the electro-optic experimental setup. (c) Dynamics of electro-optic response in E7 and E7+*h*CNTs filled test cells. The driving modulated square wave voltage profile with f = 20 Hz is shown on the right-hand y-axis. The left-hand y-axis represents the normalized transmitted intensity as a function of time as V is turned off (at t = 0) and then turned on (at t = 25 ms), for the two test cells, listed in the legend at T = 25° C.

Table 1 reveals a slight decrease (~4%) in τ_{on} for the E7+hCNT sample, whereas τ_{off} exhibits a significant acceleration (~25%) for the E7+hCNT sample, as corroborated by Figure 5 (c). This enhancement in switching response is primarily attributed to the substantial reduction in γ_1 in the E7+hCNT system. In this experiment, $V_{th} \approx 0.90$ V and the driving voltage, $|V| = 25$ V, ensuring $V >> V_{th}$. Under such high-voltage conditions, the electro-optic switching operates in the transient nematic relaxation mode, where τ_{off} is inherently fast (~ milliseconds), even for large cell gaps [73,74]. Furthermore, since $V >> V_{th}$, the driving voltage predominantly dictates τ_{on}, as indicated by Equation (5), resulting in a minimal change in τ_{on} for the E7+hCNT sample compared to pure E7. However, upon deactivation of the driving voltage, τ_{off} is a diffusion-type relaxation, mainly governed by the elastic interactions between the LC and the planar-alignment layers and influenced by γ_1. Consequently, the observed reduction in γ_1 leads to a significantly faster τ_{off} in the E7+hCNT sample. Additionally, previous studies [58] indicate that incorporating regular CNTs into an LC can enhance W_θ. Similarly, we propose that hCNTs can also enhance W_θ, leading to a faster τ_{off} according to Eq. 5.

Table 1. The two characteristic times for the pure E7 and E7+hCNTs from Figure 5(c).

Samples	τ_{on} (μs)	τ_{off} (ms)
E7	970	2.40
E7+*h*CNTs	930	1.80

Figure 5(a) presents two micrographs of the E7+hCNTs cell under a crossed-polarized microscope, capturing its voltage-off and voltage-on states. The micrograph of the voltage-off state exhibits a uniform texture with no visible hCNT aggregates, confirming a homogeneous dispersion of hCNTs in the LC at the visible length scale.

 doi:10.20944/preprints202503.1164.v1

3.5. The Effect of a Higher hCNTs Concentration

As discussed earlier, all presented experiments here thus far have been conducted at an hCNT concentration of 3.1 × 10^{-3} wt.% in E7. A key question that arises is how the ion-trapping phenomenon is affected by an increase in hCNT concentration. To investigate this, we prepared an additional sample with an hCNT concentration of 6.4 × 10^{-3} wt.% in E7, referred to as E7+hCNTs-2. Experimental results indicate that the ion-trapping efficiency at this higher concentration remains largely unchanged, with only a ±4% variation observed over the studied temperature range.

However, a distinct and intriguing phenomenon was observed at this elevated concentration. It is well established that when conventional CNTs are dispersed as colloidal inclusions in an LC medium, their long axes align along the nematic director [48–51]. We propose that this alignment mechanism also holds for hCNTs. Upon application of an external electric field, the nematic director reorients along the field direction, and due to their embedding within the nematic matrix, the hCNTs follow this field-induced director rotation.

As the hCNTs begin to rotate under the applied field, they exhibit a natural tendency to form wire-like aggregates due to entanglement. At sufficiently high concentrations, such as in E7+hCNTs-2, these hCNT-wires become significantly extended. Eventually, under a sufficiently high electric field, the elongated hCNT-wires bridge the two electrodes of the LC cell (separated by 20 μm), leading to an insulator-to-conductor transition. Figure 6 presents ε as a function of V_{rms} for E7+hCNTs-2. After reaching a maximum value, ε decreases to zero, indicating that the LC cell capacitor has been shorted.

This insulator-to-conductor transition of the LC cell is a reversible process. When the applied field is reduced to zero, the LC cell regains its original capacitance, as illustrated in the voltage up/down cycle shown in Figure 6. These findings suggest that 3.1 × 10^{-3} wt.% represents an optimal hCNT concentration for stable LC operation. Any concentration approaching or exceeding 6.4 × 10^{-3} wt.% leads to excessive hCNT aggregation, ultimately shorting the cell and preventing normal device functionality.

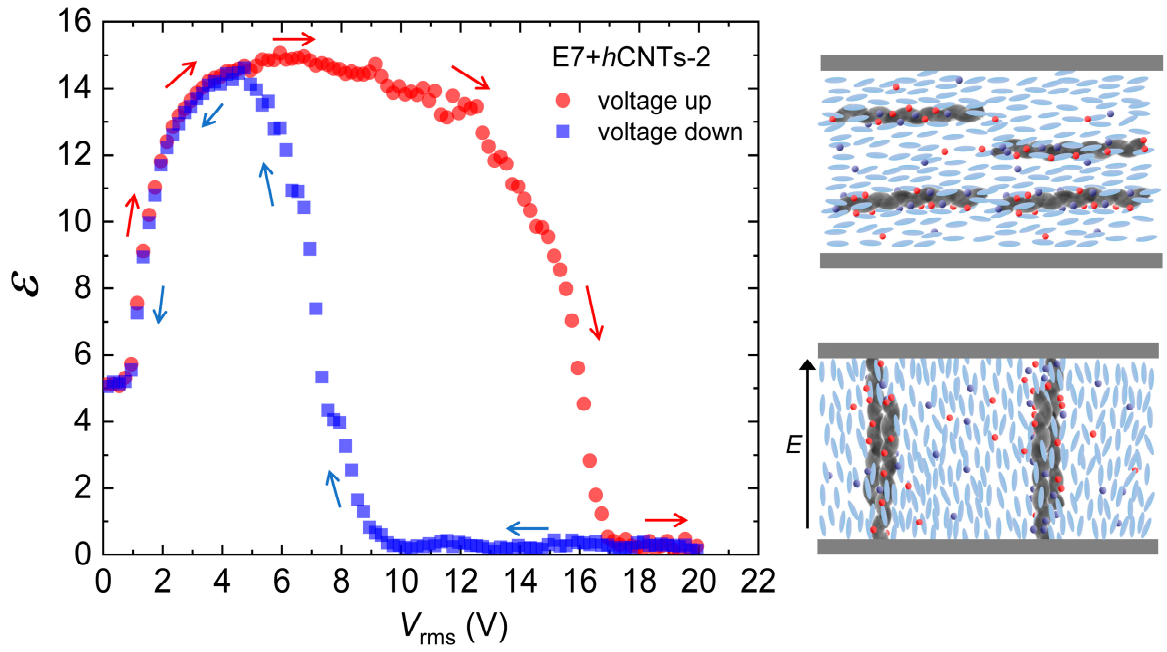

Figure 6. Dielectric constant, ε as a function of V_{rms} (voltage cycle up and down) for E7+*h*CNTs-2 at T = 25°C. Schematic representation of the presence of *h*CNTs in the LC when the field is off and the construction of *h*CNT-wires bridging the two electrodes of the cell at a high field.

 doi:10.20944/preprints202503.1164.v1

5. Conclusions

In this study, we have experimentally demonstrated that the incorporation of a small concentration of hCNTs into an LC medium effectively reduces the free ion concentration via an ion-trapping mechanism. The resulting decrease in mobile ion density lowers the internal friction within the nematic phase, thereby facilitating faster reorientation of the nematic director under an applied electric field. However, when the hCNT concentration exceeds a critical threshold (optimal concentration), the intrinsic entanglement tendency of hCNTs leads to the formation of wire-like aggregates, which ultimately short the LC cell.

These findings are significant for mitigating excess ionic impurities in LC materials and highlight the existence of an optimal hCNT concentration that balances ion trapping and electro-optic stability. The observed enhancement in optical switching speed is primarily attributed to the reduction in free ion density. This work provides valuable insights into the development of high-performance electro-optic devices based on nanostructured LC composites, offering a potential pathway toward faster and more efficient display and photonic applications.

Author Contributions: Conceptualization, R.B.; methodology, R.B. and C.C.K; software, R.B. and C.C.K; validation, R.B. and C.C.K.; formal analysis, R.B. and C.C.K investigation, R.B. and C.C.K; resources, R.B. and C.C.K.; data curation, R.B. and C.C.K; writing—original draft preparation, R.B.; writing—review and editing, R.B. and C.C.K; visualization, R.B. and C.C.K; supervision, R.B.; project administration, R.B.; funding acquisition, R.B. All authors have read and agreed to the published version of the manuscript.

Funding: This research was funded by the Office of Naval Research (Program: Nano-engineered Materials, Award No. N0001424WX01991)

Data Availability Statement: The data that support the findings of this study are available from the corresponding author, R. Basu, upon reasonable request.

References

1. Heilmeier, G. H.; Heyman, P. M. Note on Transient Current Measurements in Liquid Crystals and Related Systems. *Phys. Rev. Lett.* **1967**, *18*, 583-585.
2. Briere, G.; Gaspard, F.; Herino, R. Ionic residual conduction in the isotropic phase of a nematic liquid crystal. *Chem. Phys. Lett.* **1971**, *9*, 285-288.
3. Takahashi, S. The investigation of a dc induced transient optical 30-Hz element in twisted nematic liquid-crystal displays. *J. Appl. Phys.* **1991**, *70*, 5346-5340.
4. Vleeschouwer, H. De.; Verweire, B.; D'Have, K.; Zhang, H. Electrical and Optical Measurements of the Image Sticking Effect in Nematic LCD'S. *Mol. Cryst. Liq. Cryst.* **1999**, *331*, 567-574.
5. Vleeschouwer, H. De.; Bougrioua, F.; Pauwels, H. Importance of Ion Transport in Industrial LCD Applications, *Mol. Cryst. Liq. Cryst.* **2001**, *360*, 29-39.
6. Xu, D.; Peng, F.; Chen, H.; Yuan, J.; Wu, S.-T.; Li, M.-C.; Lee, S.-L.; Tsai, W.-C. Image sticking in liquid crystal displays with lateral electric fields. J. Appl. Phys. **2014**, *116*, 193102.
7. Vleeschouwer, H. De.; Verschueren, A.; Bougrioua, F.; Asselt, R. van; Alexander, E.; Vermael, S.; Neyts, K.; Pauwels, H. Long-term Ion Transport in Nematic Liquid Crystal Displays. *Jpn. J. Appl. Phys.* **2001,** *40*, 3272-3276.
8. Yang, K. H. Charge retention of twisted nematic liquid-crystal displays. *J. Appl. Phys.* **1990**, *67*, 36-39.
9. Sasaki, N. A. New Measurement Method for Ion Density in TFT-LCD Panels. *Mol. Cryst. Liq. Cryst.* **2001**, *367*, 671-679.
10. Murakami, S.; Naito, H. Charge Injection and Generation in Nematic Liquid Crystal Cells. *Jpn. J. Appl. Phys.* **1997**, *36*, 773-776.
11. Naemura, S.; Sawada A. Ion Generation in Liquid Crystals under Electric Field. *Mol. Cryst. Liq. Cryst.* **2000**, *346*, 155-168.
12. Van Aerle, N. A. J. M. Influence of Polyimide Orientation Layer Material on the Liquid Crystal Resistivity in LCDs. *Mol. Cryst. Liq. Cryst.* **1994**, *257*, 193-208.

 doi:10.20944/preprints202503.1164.v1

13. Sierakowski, M. Ionic interface-effects in electro-optical LC-cells. *Mol. Cryst. Liquid Cryst.* **2002**, *375*, 659–677.
14. Neyts, K.; Vermael, S.; Desimpel, C.; Stojmenovik, G.; Asselt, R. van; Verschueren, A. R. M.; de Boer, D. K. G.; Snijkers, R.; Machiels, P.; Brandenburg, A. van. Lateral ion transport in nematic liquid-crystal devices. *J. Appl. Phys.* **2003**, *94*, 3891-3896.
15. Yamashita, M.; Amemiya, Y. Drift Mobility of Positive Ions in Nematic MBBA at Low Electric Field. *Jpn. J. Appl. Phys.* **1978**, *17*, 1513-1517.
16. Novotny, V. Measurement of mobilities of particles in liquids by optical and electrical transients. *J. Appl. Phys.* **1979**, *50*, 2787-2794.
17. Sugimura, A.; Matsui, N.; Takahashi, Y.; Sonomura, H.; Naito, H.; Okuda, M. Transient currents in nematic liquid crystals. *Phys. Rev. B* **1991**, *43*, 8272-8276.
18. Naito, H.; Okuda, M.; Sugimura, A. Transient discharging processes in nematic liquid crystals. *Phys. Rev. A* **1991**, *44*, R3434-3497.
19. Naito, H.; Yoshida, K.; Okuda, M. Transient charging current in nematic liquid crystals. *J. Appl. Phys.* **1993**, *73*, 1119-1125.
20. Colpaert, C.; Maximus, B.; Meyere, A. De. Adequate measuring techniques for ions in liquid crystal layers. *Liq. Cryst.* **1996**, *21*, 133-142.
21. Sawada, A.; Manabe, A.; Nameura, S. A Comparative Study on the Attributes of Ions in Nematic and Isotropic Phases. *Jpn. J. Appl. Phys.* **2001**, *40*, 220-224.
22. Garbovskiy, Y.; Glushchenko, I. Nano-Objects and Ions in Liquid Crystals: Ion Trapping Effect and Related Phenomena. *Crystals*. **2015**, *5*, 501-533.
23. Kumar, S. *Liquid Crystals: Experimental Studies of Physical Properties and Phase Transitions*, 1st ed.; Cambridge University Press: Cambridge, UK, 2000.
24. Keller, P.; Liebert, L. Liquid crystal synthesis for physicists. In *Liquid Crystals*; Supplement 14; Liebert, L., Ed.; Academic Press: New York, NY, USA, 1978; pp. 20–75.
25. Haberfeld, J. L.; Hsu, E. C.; Johnson, J.F. Liquid crystal purification by zone refining. *Mol. Cryst. Liquid Cryst*. **1973**, *24*, 1–5.
26. Gaspard, F.; Herino, R.; Mondon, F. Low Field Conduction of Nematic Liquid Crystals Studied by Means of Electrodialysis. *Mol. Cryst. Liquid Cryst.* **1973**, *24*, 145–161.
27. Garbovskiy, Y.; Glushchenko, I.; Ion trapping by means of ferroelectric nanoparticles, and the quantification of this process in liquid crystals. *Appl. Phys. Lett.* **2015,** 107, 041106.
28. Basu, R.; Garvey, A. Effects of ferroelectric nanoparticles on ion transport in a liquid crystal. *Appl. Phys. Lett.* **2014**, *105*, 151905.
29. Ha, Y.-S.; Kim, H.-J.; Park, H.-G.; Seo, D.-S. Enhancement of electro-optic properties in liquid crystal devices via titanium nanoparticle doping. *Opt. Express* **2012**, *20*, 6448-6455.
30. Lee, C.-W.; Shih, W.-P. Quantification of ion trapping effect of carbon nanomaterials in liquid crystals. *Mater. Lett.* **2010**, *64*, 466-668.
31. Chen, H. Y.; Lee, W.; Clark, N. A. Faster electro-optical response characteristics of a carbon-nanotube-nematic suspension. *Appl. Phys. Lett.* **2007**, *90*, 033510.
32. Basu, R. Effect of carbon nanotubes on the field-induced nematic switching, *Appl. Phys. Lett.* **2013**, *103*, 241906.
33. Basu, R. Effects of graphene on electro-optic switching and spontaneous polarization of a ferroelectric liquid crystal. *Appl. Phys. Lett.* **2014**, *105*, 112905.
34. Basu, R.; Garvey, A.; Kinnamon, D. Effects of graphene on electro-optic response and ion-transport in a nematic liquid crystal. *J. Appl. Phys.* **2015**, *117*, 074301.
35. Wu, P.-W.; Lee, W. Phase and dielectric behaviors of a polymorphic liquid crystal doped with graphene nanoplatelets. *Appl. Phys. Lett.* **2013**, *102*, 162904.
36. Wu, P.-C; Lisetski, L.N.; Lee, W. Suppressed ionic effect and low-frequency texture transitions in a cholesteric liquid crystal doped with graphene nanoplatelets. *Opt. Express* **2015**, *23*, 11195-11204.

 doi:10.20944/preprints202503.1164.v1

37. Singh, D. P.; Gupta, S. K.; Vimal, T.; Manohar, R. Dielectric, electro-optical, and photoluminescence characteristics of ferroelectric liquid crystals on a graphene-coated indium tin oxide substrate. *Phys. Rev. E* **2014**, *90*, 022501.
38. Lee, W.; Wang, C.-Y.; Shih, Y.-C. Effects of carbon nanosolids on the electro-optical properties of a twisted nematic liquid-crystal host. *Appl. Phys. Lett.* **2004**, *85*, 513.
39. Shukla, R. K.; Raina, K. K.; Haase, W. Fast switching response and dielectric behavior of fullerene/ferroelectric liquid crystal nanocolloids. *Liq. Cryst.* **2014**, *41*, 1726-1732.
40. Basu, R.; Gess, D. Ion trapping, reduced rotational viscosity, and accelerated electro-optic response characteristics in gold nano-urchin--nematic suspensions, *Phys. Rev. E* **2023**, *107*, 024705.
41. Basu, R.; Lee, A. Ion trapping by the graphene electrode in a graphene-ITO hybrid liquid crystal cell. *Appl. Phys. Lett.* **2017**, *111*, 161905.
42. Basu, R.; Atwood, L. Reduced ionic effect and accelerated electro-optic response in a 2D hexagonal boron nitride planar-alignment agent based liquid crystal device. *Opt. Mater. Express.* **2019**, *9*, 1441-1449.
43. Basu, R. Reduced ionic effects and enhanced spontaneous polarization in a ferroelectric liquid crystal device employing a two-dimensional hexagonal boron nitride planar-alignment agent. *Phys. Rev. E* **2025**, *111*, 025402.
44. Li, Y.; Xu, Z.; Jia, A.;Yang, X.; Feng, W.; Wang, P.; Li, K.; Lei, W.; He, H.; Tian, Y.; Zhou, Z. Controllable modification of helical carbon nanotubes for high-performance microwave absorption. *Nanotechnol. Rev.* **2021**, *10*, 671-679.
45. Vijayan, R.; Ghazinezami, A.; Taklimi, S. R.; Khan, M. Y.; Askari, D. The geometrical advantages of helical carbon nanotubes for high-performance multifunctional polymeric nanocomposites, *Composites Part B: Engineering*. **2019**, *156*, 28-42.
46. Liu, M.; Cowley, J. M. Structures of the helical carbon nanotubes. *Carbon*. **1994**, *32*, 393-403.
47. Park, K. A.; Lee, S. M.; Lee, S. H.; Lee, Y. H. Anchoring a Liquid Crystal Molecule on a Single-Walled Carbon Nanotube. *J. Phys. Chem. C*. **2007**, **111**, 1620-1624.
48. Lynch M. D.; Patrick, D. L. Organizing Carbon Nanotubes with Liquid Crystals. *Nano Lett*. **2002**, *2*, 1197-1201.
49. Dierking, I.; Scalia, G.; Morales, P. Liquid crystal–carbon nanotube dispersions. *J. Appl. Phys.* **2005**, *97*, 044309.
50. Basu, R.; Iannacchione, G. S. Orientational coupling enhancement in a carbon nanotube dispersed liquid crystal. *Phys. Rev. E.* **2010**, *81*, 051705.
51. Basu, R.; Garvey, A. Insulator-to-conductor transition in liquid crystal-carbon nanotube nanocomposites. *J. Appl. Phys*. **2016**, *120*, 164309.
52. Basu, R.; Iannacchione, G. S. Nematic anchoring on carbon nanotubes. *Appl. Phys. Lett.* **2009**, *95*, 173113.
53. Basu, R.; Boccuzzi, K.; Ferjani, S.; Rosenblatt, C. Carbon nanotube induced chirality in an achiral liquid crystal. *Appl. Phys. Lett.* **2010,** *97*, 121908.
54. Basu, R.; Petschek, R. G.; Rosenblatt, C. Nematic electroclinic effect in a carbon nanotube doped achiral liquid crystal. *Phys. Rev. E* **2011**, *83*, 041707.
55. Kalakonda, P.; Basu, R.; Nemitz, I. R.; Rosenblatt, C.; Iannacchione, G. S. Studies of nanocomposites of carbon nanotubes and a negative dielectric anisotropy liquid crystal. *J. Chem. Phys.* **2014**, *140*, 104908.
56. Basu, R.; Chen, C.-L.; Rosenblatt, C. Carbon nanotube-induced macroscopic helical twist in an achiral nematic liquid crystal. *J. Appl. Phys.* **2011**, *109*, 083518.
57. Basu, R.; Rosenblatt, C.; Lemieux, R. Chiral induction in thioester and oxoester liquid crystals by dispersed carbon nanotubes. *Liq. Cryst.* **2012**, *39*, 199-204.
58. Lu, Y.; Chien, L. C.; Carbon nanotube doped liquid crystal OCB cells: physical and electro-optical properties. *Opt. Express*. **2008**, *16*, 12777–12785.
59. Basu, R.; Atwood, L. Homeotropic liquid crystal device employing vertically aligned carbon nanotube arrays as the alignment agent. *Phys. Rev. E.* **2020**,*102*, 022701.
60. **Basu, R.;** *Gess, D.* Electro-optic hybrid aligned nematic device utilizing carbon nanotube arrays and two-dimensional hexagonal boron nitride nanosheet as alignment substrates. *Phys. Rev. E.* **2021**, *104*, 054702.

 doi:10.20944/preprints202503.1164.v1

61. Zou, Z.; Clark, N. A.; Handschy, M. A. Ionic transport effects in SSFLC cells. *Ferroelectrics* **1991**, 121, 147-158.
62. Gennes, P. G. De; Prost, J. *The Physics of Liquid Crystals*, 1st ed.; Oxford University Press: New York, USA, 1994.
63. Liu, H.-H.; Lee; W. Ionic properties of liquid crystals dispersed with carbon nanotubes and montmorillonite nanoplatelets. *Appl. Phys. Lett.* **2010**, *97*, 173501.
64. Shukla, R. K.; Raina, K. K.; Haase, W. Fast switching response and dielectric behaviour of fullerene/ferroelectric liquid crystal nanocolloids. *Liquid Cryst.* **2014**, *41*, 1726–1732.
65. Imai, M.; Naito, H.; Okuda, M.; Okuda, M.; Sugimura, A. Determination of rotational viscosity of nematic liquid crystals from transient current numerical analysis and experiment, *Jpn. J. Appl. Phys.*, **1994**, *33*, 3482-3487.
66. Imai, M.; Naito, H.; Okuda, M.; Sugimura, A. Determination of rotational viscosity and pretilt angle in nematic liquid crystals from transient current influence of ionic conduction, *Molecular Crystals and Liquid Crystals Science and Technology. Section A.* **1995**, *259*, 37-46.
67. Imai, M.; Naito, H.; Okuda M.; Sugimura, A. A method for determination of rotational viscosity and pretilt angle from transient current in twisted nematic liquid crystal cells. *Jpn. J. Appl. Phys.* **1995**, *34*, 3170-3176.
68. Rastogi, A.; Pandey, F.; Manohar, R.; Singh, S. Effect of Doping of Cd1_xZnxS/ZnS Core/Shell Quantum Dots in Negative Dielectric Anisotropy Nematic Liquid Crystal p-Methoxybenzylidene p-Decylaniline. *Crystals*. **2021**, *11*, 605.
69. Basu, R.; Atwood, L. J.; Sterling, G. W. Dielectric and electro-optic effects in a nematic liquid crystal doped with *h*-BN flakes. *Crystals.* **2020**, *10*, 123.
70. Demus, D.; Goodby, J.; Gary, G. W.; Spiess, H.-W.; Vill, V. *Physical Properties of Liquid Crystals,* 1st ed.; Wiley VCH: Weinheim, Germany, 1999.
71. Yadav, G.; Katiyar, R.; Pathak, G.; Manohar, R.; Effect of ion trapping behavior of TiO2 nanoparticles on different parameters of weakly polar nematic liquid crystal. *J. Theor. Appl. Phys.* **2018**, *12*, 191–198.
72. Nie, X.; Lu, R.; Xianyu, H.; Wu, T.X.; Wu, S.T. Anchoring energy and cell gap effects on liquid crystal response time. *J. Appl. Phys.* **2007**, *101*, 103110.
73. Wu, S.T.; Wu, C.S. High-speed liquid-crystal modulators using transient nematic effect. *J. Appl. Phys.* **1989**, *65*, 527-532.
74. Wu, S.T.; Wu, C.S. Small angle relaxation of highly deformed nematic liquid crystals. *Appl. Phys. Lett.* **1988**, *53*, 1794-1796.